Tomographic reconstruction of atmospheric turbulence with the use of time-dependent stochastic inversion

Sergey N. Vecherin
Department of Physics, New Mexico State University, Las Cruces, New Mexico 88003

Vladimir E. Ostashev
NOAA/Earth System Research Laboratory, Boulder, Colorado 80305 and Department of Physics, New Mexico State University, Las Cruces, New Mexico 88003

A. Ziemann
University of Leipzig, Institute for Meteorology, Stephanstrasse 3, 04103 Leipzig, Germany

D. Keith Wilson
U.S. Army Engineer Research and Development Center, Hanover, New Hampshire 03755

K. Arnold
University of Leipzig, Dezernat 2, Goethestr. 6, 04109 Leipzig, Germany

M. Barth
University of Leipzig, Institute for Meteorology, Stephanstr. 3, 04103 Leipzig, Germany

(Received 16 November 2006; revised 14 June 2007; accepted 18 June 2007)

Acoustic travel-time tomography allows one to reconstruct temperature and wind velocity fields in the atmosphere. In a recently published paper [S. Vecherin *et al.*, J. Acoust. Soc. Am. **119**, 2579 (2006)], a time-dependent stochastic inversion (TDSI) was developed for the reconstruction of these fields from travel times of sound propagation between sources and receivers in a tomography array. TDSI accounts for the correlation of temperature and wind velocity fluctuations both in space and time and therefore yields more accurate reconstruction of these fields in comparison with algebraic techniques and regular stochastic inversion. To use TDSI, one needs to estimate spatial-temporal covariance functions of temperature and wind velocity fluctuations. In this paper, these spatial-temporal covariance functions are derived for locally frozen turbulence which is a more general concept than a widely used hypothesis of frozen turbulence. The developed theory is applied to reconstruction of temperature and wind velocity fields in the acoustic tomography experiment carried out by University of Leipzig, Germany. The reconstructed temperature and velocity fields are presented and errors in reconstruction of these fields are studied. © *2007 Acoustical Society of America.* [DOI: 10.1121/1.2756798]

PACS number(s): 43.28.We, 43.28.Vd, 43.20.Dk [RR] Pages: 1416–1425

I. INTRODUCTION

Knowledge about temperature and wind velocity fields is important in many disciplines, e.g. boundary layer meteorology, theories of turbulence, and studies of electromagnetic and acoustic wave propagation in the atmosphere. A conventional way to measure the temperature and wind velocity is to use *in situ* sensors. However, such measurements can provide the data only at some spatial points. To measure the temperature and velocity fields with high resolution, a very large number of sensors is required. This will not only increase the cost of measurements but also distort the original fields. This problem can be overcome by using acoustic tomography.

Acoustic travel-time tomography of the atmosphere allows one to reconstruct temperature $\tilde{T}(\mathbf{R})$ and wind velocity $\tilde{\mathbf{V}}(\mathbf{R})$ fields in a tomographic volume or area given positions of sound sources and receivers and travel times t_i^{tr} of sound propagation between them. Here, $\mathbf{R}=(x,y,z)$ is a vector in the Cartesian coordinate system and $i=1,2,\ldots,I$, where I is the number of data t_i^{tr}, i.e., the number of sound propagation paths between sources and receivers.

In the past decade, several acoustic travel-time tomography experiments have been carried out in the lowermost few meters of the atmosphere.[1–9] Further, some works were done on numerical simulation of acoustic tomography of the atmosphere.[10–13] One of the main problems in both tomography experiments and numerical simulations is to find a good inverse algorithm for reconstruction of $\tilde{T}$ and $\tilde{\mathbf{V}}$ fields. Most of the algorithms used so far employed a partition of a tomographic volume into grid cells where the values of $\tilde{T}$ and $\tilde{\mathbf{V}}$ are constant, and a subsequent solution of a set of algebraic equations.[3–9,11,12,14,15] Numerical simulations have shown[12] that these algebraic algorithms can give a good reconstruction of $\tilde{T}$ and $\tilde{\mathbf{V}}$ fields if the number of the grid cells is small enough so that a corresponding inverse problem is overdetermined (the number of equations is greater than the number of unknowns). However, in two-dimensional (2D)

Report Documentation Page

Form Approved
OMB No. 0704-0188

1. REPORT DATE	2. REPORT TYPE	3. DATES COVERED
27 AUG 2007	**N/A**	**-**

4. TITLE AND SUBTITLE	5a. CONTRACT NUMBER
Tomographic Reconstruction of Atmospheric Tturbulence with the Use of Time-Dependent Stochastic Inversion	5b. GRANT NUMBER
	5c. PROGRAM ELEMENT NUMBER
6. AUTHOR(S)	5d. PROJECT NUMBER
	5e. TASK NUMBER
	5f. WORK UNIT NUMBER
7. PERFORMING ORGANIZATION NAME(S) AND ADDRESS(ES) **Physics Department New Mexico State University Box 3001, Dept 3D Las Cruces, NM 88003**	8. PERFORMING ORGANIZATION REPORT NUMBER
9. SPONSORING/MONITORING AGENCY NAME(S) AND ADDRESS(ES)	10. SPONSOR/MONITOR'S ACRONYM(S)
	11. SPONSOR/MONITOR'S REPORT NUMBER(S)

12. DISTRIBUTION/AVAILABILITY STATEMENT
Approved for public release, distribution unlimited

13. SUPPLEMENTARY NOTES
Govt. rights, The original document contains color images.

14. ABSTRACT

15. SUBJECT TERMS

16. SECURITY CLASSIFICATION OF:			17. LIMITATION OF ABSTRACT	18. NUMBER OF PAGES	19a. NAME OF RESPONSIBLE PERSON
a. REPORT	b. ABSTRACT	c. THIS PAGE			
unclassified	**unclassified**	**unclassified**	**SAR**	**10**	

tomography experiments, for example, there are three continuous fields to reconstruct (temperature and two components of velocity), whereas the number of data is limited. (A large number of sources and receivers can distort the $\tilde{T}$ and $\tilde{\mathbf{V}}$ fields inside a tomographic area.) Therefore, the number of grid cells where $\tilde{T}$ and $\tilde{\mathbf{V}}$ are reconstructed is relatively small (a few dozen or less).

To increase spatial resolution of the reconstructed temperature $\tilde{T}$ and velocity $\tilde{\mathbf{V}}$ fields, one can use a stochastic inversion (SI), which is appropriate for solutions of inverse problems involving continuous fields.[2,16] In SI, the increase in spatial resolution comes with a price: One needs to know spatial covariance functions $B_{TT}^{s}(\mathbf{R}_1,\mathbf{R}_2)$ and $B_{ij}^{s}(\mathbf{R}_1,\mathbf{R}_2)$ of temperature and velocity fluctuations at the time moment t of an experiment. Here, s stands for spatial, and i and j indicate the components of wind velocity vector. Recent studies have shown[13,17] that, in SI, the use of different covariance functions (exponential, Gaussian, von Kármán, and some others) results in the reconstructed temperature and velocity fields which are nearly identical (with a relationship between correlation lengths that provides the equality of the integral lengths of these functions, see Ref. 18 for details). Therefore, one of these covariance functions, e.g., Gaussian, can be used in SI. Note that in SI the accuracy of $\tilde{T}$ and $\tilde{\mathbf{V}}$ reconstruction increases with the increase of the number I of data.

To increase the number of data without increasing the number of sources and receivers, a time-dependent stochastic inversion (TDSI) in acoustic tomography of the atmosphere was proposed in Ref. 19. In TDSI, the travel times t_i^{tr} are measured repeatedly at the time moments $t_1,t_2,\ldots,t_n$. Then, the fields $\tilde{T}(\mathbf{R},t)$ and $\tilde{\mathbf{V}}(\mathbf{R},t)$ are reconstructed given n sets of t_i^{tr}, positions of sources and receivers, and assuming that the spatial-temporal covariance functions of temperature and wind velocity fluctuations, $B_{TT}(\mathbf{R}_1,t_1;\mathbf{R}_2,t_2)$ and $B_{ij}(\mathbf{R}_1,t_1;\mathbf{R}_2,t_2)$, are known. In Ref. 19, these spatial-temporal covariance functions were determined assuming that turbulence is frozen,[20] i.e., temperature and wind velocity fluctuations are advected with the constant wind velocity $\mathbf{V}_0$. Numerical simulation of acoustic tomography of the atmosphere showed that TDSI allows better reconstruction of temperature and velocity fields than SI does.[19]

A general idea to use spatial-temporal covariances in SI is known in the literature. For example, this idea has been successfully used in the satellite altimetry of the ocean surface level.[21–23] TDSI in acoustic tomography of the atmosphere is somewhat similar to methods used in the satellite altimetry. However, a mathematical apparatus of TDSI is different from that used in altimetry and was developed in Ref. 19.

The main goal of the present paper is further development of a mathematical apparatus of TDSI and the use of the developed theory in the reconstruction of the $\tilde{T}$ and $\tilde{\mathbf{V}}$ fields in the acoustic tomography experiment STINHO (STructure of turbulent transport under INHOmogeneous surface conditions) carried out by University of Leipzig, Germany.[9] First, we derive analytical formulas for $B_{TT}(\mathbf{R}_1,t_1;\mathbf{R}_2,t_2)$ and $B_{ij}(\mathbf{R}_1,t_1;\mathbf{R}_2,t_2)$ for the case of locally frozen turbulence which is a generalization of the hypothesis of frozen turbulence. The obtained formulas for $B_{TT}(\mathbf{R}_1,t_1;\mathbf{R}_2,t_2)$ and $B_{ij}(\mathbf{R}_1,t_1;\mathbf{R}_2,t_2)$ account for the variance of wind velocity fluctuations σ_V and, hence, are much more realistic than those for the case of frozen turbulence where σ_V is tacitly assumed 0. Second, we determine errors in the input data for TDSI. Finally using these errors and formulas for $B_{TT}(\mathbf{R}_1,t_1;\mathbf{R}_2,t_2)$ and $B_{ij}(\mathbf{R}_1,t_1;\mathbf{R}_2,t_2)$ for locally frozen turbulence, we apply TDSI for reconstruction of $\tilde{T}$ and $\tilde{\mathbf{V}}$ fields in the acoustic tomography experiment STINHO. Note that this is the first reconstruction of the temperature and wind velocity fields in an acoustic tomography of the atmosphere experiment using TDSI.

The paper is organized as follows. Section II describes starting equations for acoustic tomography and the TDSI algorithm. Formulas for spatial-temporal covariance functions of temperature and wind velocity fluctuations for locally frozen turbulence are derived in Sec. III. Using the residual analysis, the errors in the input data for TDSI are obtained in Sec. IV. In Sec. V, new methodology is applied to reconstruction of temperature and velocity fields in the acoustic tomography experiment STINHO. The conclusions are presented in Sec. VI.

II. STARTING EQUATIONS

In this section, starting equations for acoustic travel-time tomography of the atmosphere and a brief description of TDSI are presented. A detailed description of TDSI can be found in Ref. 19.

Let $\tilde{u}(\mathbf{R},t)$, $\tilde{v}(\mathbf{R},t)$, and $\tilde{w}(\mathbf{R},t)$ be x, y, and z components of the random, three-dimensional (3D) vector of wind velocity $\tilde{\mathbf{V}}(\mathbf{R},t)$:

$$\tilde{\mathbf{V}}(\mathbf{R},t)=\tilde{u}(\mathbf{R},t)\mathbf{e}_x+\tilde{v}(\mathbf{R},t)\mathbf{e}_y+\tilde{w}(\mathbf{R},t)\mathbf{e}_z. \tag{1}$$

Here $\mathbf{e}_x$, $\mathbf{e}_y$, and $\mathbf{e}_z$ are the unit vectors along the x, y, and z axes, respectively. The adiabatic sound speed c_L, temperature $\tilde{T}$, and wind velocity $\tilde{\mathbf{V}}$ within a tomographic area at the time moment t can be represented as sums of their spatially averaged values $c_0(t)$, $T_0(t)$, $\mathbf{V}_0(t)=(u_0(t),v_0(t),w_0(t))$ and their fluctuations $c(\mathbf{R},t),T(\mathbf{R},t),\mathbf{V}(\mathbf{R},t)=(u(\mathbf{R},t),v(\mathbf{R},t),w(\mathbf{R},t))$:

$$c_L(\mathbf{R},t)=c_0(t)+c(\mathbf{R},t),\tilde{T}=T_0(t)+T(\mathbf{R},t),$$
$$\tilde{\mathbf{V}}(\mathbf{R},t)=\mathbf{V}_0(t)+\mathbf{V}(\mathbf{R},t). \tag{2}$$

Note that tomography allows one to reconstruct *acoustic virtual* temperature, which we denote as $\tilde{T}$. It is related to the thermodynamic temperature T_{th} by the following relationship: $\tilde{T}\cong T_{\mathrm{th}}(1+0.511q)$, where q is the specific humidity of air.[18]

We will assume that the spatially averaged values are equal to the mathematical expectations of the random fields at each spatial point at the time moment t, i.e.,

$$\langle c_L(\mathbf{R},t)\rangle = c_0(t), \quad \langle \tilde{T}(\mathbf{R},t)\rangle = T_0(t), \quad \langle \tilde{\mathbf{V}}(\mathbf{R},t)\rangle = \mathbf{V}_0(t). \tag{3}$$

Hereinafter, the angular brackets $\langle\ \rangle$ denote averaging over an ensemble of realizations. Note that it follows from Eqs. (2) and (3) that the mathematical expectations of the fluctuations at any point $\mathbf{R}$ and time t are equal to zero.

Most acoustic tomography arrays used so far were 2D. In Ref. 19 TDSI was developed for the 2D case in which sources, receivers, and sound propagation paths are located in one plane. For concreteness, we will assume that this plane coincides with the (x,y) plane. In this case, the travel times of sound propagation between sources and receivers are given by linearized equations of the forward problem of acoustic travel-time tomography of the atmosphere[19]:

$$t_i^{\mathrm{tr}}(t) = \frac{L_i}{c_0(t)}\left(1 - \frac{u_0(t)s_{xi} + v_0(t)s_{yi}}{c_0(t)}\right) - \frac{1}{c_0^2(t)} \times \int_{L_i} dl\left\{\frac{c_0(t)}{2T_0(t)}T(\mathbf{R},t) + u(\mathbf{R},t)s_{xi} + v(\mathbf{R},t)s_{yi}\right\}. \tag{4}$$

Here L_i is the distance between a source and receiver, $s_{xi} = \cos\varphi_i$, and $s_{yi} = \sin\varphi_i$, where φ_i is the angle between $\mathbf{e}_x$ and the direction of sound propagation. Note that in the linearized forward problem the paths of sound impulses can be approximated by straight lines.

The inverse problem of 2D acoustic travel-time tomography of the atmosphere is to reconstruct the mean fields $T_0(t)$, $u_0(t)$, $v_0(t)$ and their fluctuations $T(\mathbf{R},t)$, $u(\mathbf{R},t)$, $v(\mathbf{R},t)$ given the travel times $t_i^{\mathrm{tr}}(t)$, the angles φ_i, and the distances L_i. This reconstruction consists of two steps. First, $T_0(t)$, $u_0(t)$, and $v_0(t)$ are reconstructed using the least-squares estimation. Then, the fluctuations $T(\mathbf{R},t)$, $u(\mathbf{R},t)$, and $v(\mathbf{R},t)$ are reconstructed with the help of TDSI.

When reconstructing $T_0(t)$, $u_0(t)$, and $v_0(t)$, the integral term on the right-hand side of Eq. (4) is neglected. In this case, Eq. (4) can be rewritten in a matrix notation:

$$\mathbf{Gf} = \mathbf{b}. \tag{5}$$

Here the elements of the column-vector $\mathbf{b}$ are known (can be calculated from experimentally measured values of $t_i^{\mathrm{tr}}(t)$ and L_i):

$$b_i = \frac{t_i^{\mathrm{tr}}(t)}{L_i}, \tag{6}$$

the unknown column-vector $\mathbf{f}$ has three elements

$$f_1 = \frac{1}{c_0(t)}, \quad f_2 = \frac{u_0(t)}{c_0^2(t)}, \quad f_3 = \frac{v_0(t)}{c_0^2(t)}, \tag{7}$$

and the matrix $\mathbf{G}$ is given by

$$\mathbf{G} = \begin{bmatrix} 1 & -\cos\varphi_1 & -\sin\varphi_1 \\ \vdots & \ddots & \vdots \\ 1 & -\cos\varphi_I & -\sin\varphi_I \end{bmatrix}. \tag{8}$$

Then, the overdetermined inverse problem for the elements of vector $\mathbf{f}$ (I is assumed to be greater than 3) is solved using the least-squares estimation:

$$\hat{\mathbf{f}} = (\mathbf{G}^T\mathbf{G})^{-1}\mathbf{G}^T\mathbf{b}. \tag{9}$$

Here $\hat{\mathbf{f}}$ is the optimal least-squares estimation of $\mathbf{f}$. The optimal estimations $\hat{c}_0$, $\hat{u}_0$, $\hat{v}_0$ of the mean fields c_0, u_0, v_0 can easily be calculated from $\hat{\mathbf{f}}$ using Eq. (7). The mean temperature $\hat{T}_0$ can be obtained from $\hat{c}_0$ using the following formula:

$$c_0^2 = \gamma R_a T_0, \tag{10}$$

where $\gamma \approx 1.41$ is the ratio of the specific heats and R_a is the gas constant for dry air.

The estimated values $\hat{c}_0$, $\hat{T}_0$, $\hat{u}_0$, and $\hat{v}_0$ are substituted back into Eq. (4). The resulting equation can be written in the following form:

$$q_i(t) = \int_{L_i} dl\left\{\frac{\hat{c}_0(t)}{2\hat{T}_0(t)}T(\mathbf{R},t) + u(\mathbf{R},t)s_{xi} + v(\mathbf{R},t)s_{yi}\right\}, \tag{11}$$

where $q_i(t)$ are given by

$$q_i(t) = L_i[\hat{c}_0(t) - \hat{u}_0(t)s_{xi} - \hat{v}_0(t)s_{yi}] - \hat{c}_0^2(t)t_i^{tr}(t). \tag{12}$$

After the reconstruction of the mean fields, $q_i(t)$ are known.

Equation (11) is a starting equation for TDSI whose goal is to reconstruct $T(\mathbf{R},t)$, $u(\mathbf{R},t)$ and $v(\mathbf{R},t)$ given the values of $q_i(t)$, φ_i, and L_i. The $q_i(t)$ are known at the time moments $t_1, t_2, \ldots, t_n$ of an experiment and are used to form the vector $\mathbf{d}$ of the input data for TDSI:

$$\mathbf{d} = [\mathbf{q}(t_1); \mathbf{q}(t_2); \ldots; \mathbf{q}(t_n)]. \tag{13}$$

Here $\mathbf{q}(t_k)$ are column vectors with elements given by Eq. (12), and the semicolons indicate that these $\mathbf{q}$ are arranged in the column vector $\mathbf{d}$.

Let $\mathbf{m}(t)$ be a column vector of the fluctuations being reconstructed at certain spatial points $\mathbf{R}_1, \ldots, \mathbf{R}_J$, where J is a total number of points:

$$\mathbf{m}(t) = [T(\mathbf{R}_1,t); \ldots; T(\mathbf{R}_J,t); u(\mathbf{R}_1,t); \ldots; u(\mathbf{R}_J,t); v(\mathbf{R}_1,t); \ldots; v(\mathbf{R}_J,t)]. \tag{14}$$

Note that in TDSI the fluctuations can be reconstructed at any time moment t. Of course, one can expect a good reconstruction of $T(\mathbf{R},t)$, $u(\mathbf{R},t)$, and $v(\mathbf{R},t)$ fields if t is within the time interval $[t_1,t_n]$ or close to it. In TDSI, the optimal reconstruction $\hat{\mathbf{m}}(t)$ of $\mathbf{m}(t)$ is given by the following formula:

$$\hat{\mathbf{m}}(t) = \mathbf{C}_{\mathbf{md}}\mathbf{C}_{\mathbf{dd}}^{-1}\mathbf{d}, \tag{15}$$

where $\mathbf{C}_{\mathbf{md}} = \langle \mathbf{md}^T \rangle$ is a model-data covariance matrix and $\mathbf{C}_{\mathbf{dd}} = \langle \mathbf{dd}^T \rangle$ is a data covariance matrix given by Eqs. (18)–(21) from Ref. 19. The elements of these matrices are expressed in terms of the integrals along the sound propaga-

tion paths between sources and receivers, whose integrands contain the spatial-temporal covariance functions of temperature and wind velocity fluctuations, $B_{TT}(\mathbf{R}_1,t_1;\mathbf{R}_2,t_2)$ and $B_{ij}(\mathbf{R}_1,t_1;\mathbf{R}_2,t_2)$. In an experiment, the components q_i of the vector $\mathbf{d}$ are always known with some uncertainties (observation noise) which we denote as Δ_{qi}. As a result, the matrix $\mathbf{C_{dd}}$ has additional terms on its main diagonal[19] equal to the variances of these uncertainties $\sigma_{qi}^2=\langle\Delta_{qi}^2\rangle$.

Expected squared errors of the estimation $\tilde{\mathbf{m}}(t)$ are elements on the main diagonal of the error covariance matrix $\mathbf{C}_{\boldsymbol{\epsilon\epsilon}}$, given by[19]

$$\mathbf{C}_{\boldsymbol{\epsilon\epsilon}}=\mathbf{C_{mm}}-\mathbf{C_{md}}\mathbf{C_{dd}}^{-1}\mathbf{C}_{\mathbf{md}}^{T}, \tag{16}$$

where $\mathbf{C_{mm}}=\langle\mathbf{mm}^T\rangle$ is a model covariance matrix.

Thus, in order to implement TDSI for reconstruction of temperature and wind velocity fields, one needs to know spatial-temporal covariance functions $B_{TT}(\mathbf{R}_1,t_1;\mathbf{R}_2,t_2)$ and $B_{ij}(\mathbf{R}_1,t_1;\mathbf{R}_2,t_2)$ and the variances σ_{qi}^2. These covariance functions and variance will be calculated in the next two sections.

III. LOCALLY FROZEN TURBULENCE

In this section, analytical formulas for the spatial-temporal covariance functions of temperature and wind velocity fluctuations, $B_{TT}(\mathbf{R}_1,t_1;\mathbf{R}_2,t_2)$ and $B_{ij}(\mathbf{R}_1,t_1;\mathbf{R}_2,t_2)$, are derived for the case of locally frozen turbulence.

For this derivation, we will need particular forms of the spatial covariance functions of temperature and wind velocity fluctuations $B_{TT}^s(\mathbf{R}_1,\mathbf{R}_2)$ and $B_{ij}^s(\mathbf{R}_1,\mathbf{R}_2)$. We will assume that turbulence is statistically isotropic and homogeneous, and that the spatial covariance functions of temperature and longitudinal velocity fluctuations are given by Gaussian functions. The components of the tensor $B_{ij}^s(\mathbf{R}_1,\mathbf{R}_2)$ can be calculated from the covariance function of longitudinal velocity fluctuations using Eqs. (6.34) and (6.35) in Ref. 18. As a result, we obtain the following spatial covariance functions of temperature and velocity fluctuations:

$$B_{TT}^s(\mathbf{R}_1,\mathbf{R}_2)=\sigma_T^2\exp\left(-\frac{\boldsymbol{\rho}^2}{l_T^2}\right), \tag{17}$$

$$B_{uu}^s(\mathbf{R}_1,\mathbf{R}_2)=\sigma_V^2\exp\left(-\frac{\boldsymbol{\rho}^2}{l_V^2}\right)\left(1-\frac{\rho_y^2+\rho_z^2}{l_V^2}\right), \tag{18}$$

$$B_{uv}^s(\mathbf{R}_1,\mathbf{R}_2)=\sigma_V^2\exp\left(-\frac{\boldsymbol{\rho}^2}{l_V^2}\right)\frac{\rho_x\rho_y}{l_V^2}. \tag{19}$$

Here, σ_T and σ_V are the standard deviations of temperature and velocity fluctuations, l_T and l_V are their correlation lengths, and $\boldsymbol{\rho}=\mathbf{R}_2-\mathbf{R}_1=(\rho_x,\rho_y,\rho_z)$. Other components of the tensor $B_{ij}^s(\mathbf{R}_1,\mathbf{R}_2)$ are given by formulas similar to those for $B_{uu}^s(\mathbf{R}_1,\mathbf{R}_2)$ and $B_{uv}^s(\mathbf{R}_1,\mathbf{R}_2)$.

A hypothesis of locally frozen turbulence is formulated in Ref. 24. According to this hypothesis, during a relatively small time interval τ, velocities $\tilde{\mathbf{V}}(\mathbf{R},t)$ can be considered as constant in the vicinity of each spatial point. This allows one to express the temperature field $T(\mathbf{R},t_2)$ at the time moment t_2 in terms of the temperature field at the time moment t_1:

$$T(\mathbf{R},t_2)=T(\mathbf{R}-\tilde{\mathbf{V}}(\mathbf{R},t_1)\tau,t_1), \tag{20}$$

where $\tau=t_2-t_1$. Note that in Eq. (20) the velocity $\tilde{\mathbf{V}}$ is a random function of $\mathbf{R}$ and t_1. If in Eq. (20) $\tilde{\mathbf{V}}$ were constant, this equation would become a formula for frozen turbulence which has been widely used in the literature.[20] Thus, the hypothesis of locally frozen is a generalization of that of frozen turbulence.

Equation (20) allows one to express the spatial-temporal covariance function $B_{TT}(\mathbf{R}_1,t_1;\mathbf{R}_2,t_2)$ in terms of the spatial covariance function $B_{TT}^s(\mathbf{R}_1,\mathbf{R}_2)$. Using this equation, we have:

$$\begin{aligned}B_{TT}(\mathbf{R}_1,t_1;\mathbf{R}_2,t_2)&\equiv\langle T(\mathbf{R}_1,t_1)T(\mathbf{R}_2,t_2)\rangle_{T,\tilde{\mathbf{V}}}\\&=\langle T(\mathbf{R}_1,t_1)T(\mathbf{R}_2-\tilde{\mathbf{V}}(\mathbf{R}_2,t_1)\tau,t_1)\rangle_{T,\tilde{\mathbf{V}}}.\end{aligned} \tag{21}$$

Here, $\langle\ \rangle_{T,\tilde{\mathbf{V}}}$ denotes the average over an ensemble of realizations of the random fields T and $\tilde{\mathbf{V}}$. These fields are uncorrelated in the model of homogeneous isotropic turbulence which is used in this paper.[24] Assuming Gaussian probability density distribution, these random fields are statistically independent. Therefore, in the right-hand side of Eq. (21), one can first calculate the average over an ensemble of realizations of T which yields the spatial covariance function B_{TT}^s by definition. Taking into account that $\boldsymbol{\rho}=\mathbf{R}_2-\mathbf{R}_1$, we have

$$B_{TT}(\boldsymbol{\rho},\tau)=\langle B_{TT}^s(\boldsymbol{\rho}-\tilde{\mathbf{V}}(\mathbf{R}_2,t_1)\tau)\rangle_{\tilde{\mathbf{V}}}. \tag{22}$$

The average on the right-hand side of this formula is calculated in the Appendix. The result is

$$B_{TT}(\boldsymbol{\rho},\tau)=\tilde{\sigma}_T^2\exp\left[-\frac{(\boldsymbol{\rho}-\mathbf{V}_0(t_1)\tau)^2}{\tilde{l}_T^2}\right], \tag{23}$$

where the effective variance $\tilde{\sigma}_T^2$ and the square of correlation length $\tilde{l}_T^2$ are given by

$$\tilde{\sigma}_T^2=\frac{\sigma_T^2}{\left[1+2\left(\frac{\sigma_V\tau}{l_T}\right)^2\right]^{3/2}},\quad \tilde{l}_T^2=l_T^2+2\sigma_V^2\tau^2. \tag{24}$$

Note that Eqs. (23) and (24) can also be derived from Eq. (31.29) in Ref. 24. The latter equation gives a formula for a Fourier transform of $B_{TT}(\boldsymbol{\rho},\tau)$ with respect to $\boldsymbol{\rho}$ and τ, valid for an arbitrary spatial covariance function and probability density distribution.

Similarly to the derivation of Eq. (23), one can obtain a formula for the spatial-temporal covariance function of the longitudinal velocity fluctuations and, then, formulas for $B_{uu}(\boldsymbol{\rho},t)$ and $B_{uv}(\boldsymbol{\rho},t)$:

$$\begin{aligned}B_{uu}(\boldsymbol{\rho},t)=\tilde{\sigma}_V^2\exp&\left[-\frac{(\boldsymbol{\rho}-\mathbf{V}_0(t_1)\tau)^2}{\tilde{l}_V^2}\right]\\&\times\left(1-\frac{(\rho_y-v_0(t_1)\tau)^2+(\rho_z-w_0(t_1)\tau)^2}{\tilde{l}_V^2}\right),\end{aligned} \tag{25}$$

$$B_{uv}(\boldsymbol{\rho},t)=\tilde{\sigma}_V^2\exp\left[-\frac{(\boldsymbol{\rho}-\mathbf{V}_0(t_1)\tau)^2}{\tilde{l}_V^2}\right]\times\frac{(\rho_x-u_0(t_1)\tau)(\rho_y-v_0(t_1)\tau)}{\tilde{l}_V^2},\tag{26}$$

where

$$\tilde{\sigma}_V^2=\frac{\sigma_V^2}{\left[1+2\left(\frac{\sigma_V\tau}{l_V}\right)^2\right]^{3/2}},\quad \tilde{l}_V^2=l_V^2+2\sigma_V^2\tau^2.\tag{27}$$

Equations (23)–(27) provide analytical formulas for the spatial-temporal covariance functions of temperature and velocity fluctuations for the considered case of locally frozen turbulence. In the limiting case $\sigma_V=0$ and time-independent $\mathbf{V}_0$, these formulas coincide with those for frozen turbulence.[19] It follows from Eqs. (23)–(27) that the dependence of the spatial-temporal covariance functions on τ manifests in three effects: The spatial arguments of the covariance functions are shifted by the vector $\mathbf{V}_0(t_1)\tau$, and the effective variances of the fluctuations decrease while the effective correlation lengths increase with the increase in τ.

A necessary condition of applicability of the hypothesis of locally frozen turbulence is formulated in Ref. 24:

$$\sigma_V\ll|\mathbf{V}_0|.\tag{28}$$

In this paper, we consider the case when the mean wind velocity $\mathbf{V}_0$ can slowly depend on time t. This imposes an additional necessary condition of applicability of the hypothesis of locally frozen turbulence:

$$|\mathbf{V}_0(t)-\mathbf{V}_0(t_1)|\ll|\mathbf{V}_0(t_1)|,\tag{29}$$

where $t\in[t_1,t_2]$. As far as we know sufficient conditions of applicability of the hypothesis of locally frozen turbulence have not been obtained. They should probably include a limitation on the time interval $\tau=t_2-t_1$ during which this hypothesis is valid.

IV. ESTIMATION OF THE ERRORS

In this section, the variances σ_{qi}^2 of the uncertainties Δ_{q_i} in the input data $\mathbf{d}$ are calculated. It follows from Eq. (11) that these variances depend on the variances of mean squared errors $\hat{\sigma}_c^2$, $\hat{\sigma}_T^2$, $\hat{\sigma}_u^2$, and $\hat{\sigma}_v^2$ in reconstruction of $\hat{c}_0$, $\hat{T}_0$, $\hat{u}_0$, and $\hat{v}_0$. Therefore, we first estimate these errors.

Let s_b^2 be the estimated variance of components b_i of the vector $\mathbf{b}$ which appears in the right-hand side of Eq. (5). Using a residual estimation,[16] we have

$$s_b^2=\frac{(\mathbf{b}-\mathbf{G}\hat{\mathbf{f}})^T(\mathbf{b}-\mathbf{G}\hat{\mathbf{f}})}{I-3},\tag{30}$$

where $I-3$ is a number of independent degrees of freedom in the numerator of Eq. (30). The mean squared errors $\sigma_{\hat{\mathbf{f}}}^2$ of the vector $\hat{\mathbf{f}}$ are diagonal elements of its covariance matrix[16] $\sigma_{\hat{\mathbf{f}}}^2=\mathrm{diag}[\mathbf{R}_{\hat{\mathbf{f}}\hat{\mathbf{f}}}]$. Here

$$\mathbf{R}_{\hat{\mathbf{f}}\hat{\mathbf{f}}}=s_b^2(\mathbf{G}^T\mathbf{G})^{-1}.\tag{31}$$

Using Eqs. (7) and (10) and neglecting the terms of order $(\hat{u}_0/\hat{c}_0)^2$ and $(\hat{v}_0/\hat{c}_0)^2$, the mean squared errors $\hat{\sigma}_c^2$, $\hat{\sigma}_T^2$, $\hat{\sigma}_u^2$, and $\hat{\sigma}_v^2$ can be expressed in terms of the mean squared errors $\sigma_{\hat{\mathbf{f}}}^2$:

$$\hat{\sigma}_c^2=\hat{c}_0^4\sigma_{\hat{f}_1}^2,\quad \hat{\sigma}_T^2=\frac{4\hat{c}_0^2}{(\gamma R_a)^2}\hat{\sigma}_c^2,\quad \hat{\sigma}_u^2=\hat{c}_0^4\sigma_{\hat{f}_2}^2,\quad \hat{\sigma}_v^2=\hat{c}_0^4\sigma_{\hat{f}_3}^2.\tag{32}$$

Once the errors $\hat{\sigma}_c^2$, $\hat{\sigma}_T^2$, $\hat{\sigma}_u^2$, and $\hat{\sigma}_v^2$ are known, it is possible to estimate the variances $\sigma_{q_i}^2$ of the errors in the input data $q_i(t)$ for TDSI. The errors in $q_i(t)$ are due to errors in L_i, s_{xi}, and s_{yi} caused by uncertainties in transducers positions, errors in measurements of t_i^{tr}, and errors in the reconstruction of $\hat{c}_0(t)$, $\hat{T}_0(t)$, $\hat{u}_0(t)$, and $\hat{v}_0(t)$. As $L_i^2=(x_i-x_{0i})^2+(y_i-y_{0i})^2$, where (x_i,y_i) and (x_{0i},y_{0i}) are the coordinates of the receiver and source, respectively, one can calculate the uncertainties in the sound propagation paths Δ_{L_i} taken into account that $\cos\varphi_i=(x_i-x_{0i})/L_i$ and $\sin\varphi_i=(y_i-y_{0i})/L_i$:

$$\Delta_{L_i}=[(\Delta_{x_i}-\Delta_{x_{0i}})\cos\varphi_i+(\Delta_{y_i}-\Delta_{y_{0i}})\sin\varphi_i].\tag{33}$$

Here, Δ_{x_i}, $\Delta_{x_{0i}}$, Δ_{y_i}, and $\Delta_{y_{0i}}$ are uncertainties in the transducer positions. Therefore, from Eq. (12) the uncertainty Δ_{q_i} is

$$\Delta_{q_i}=(\Delta_{x_i}-\Delta_{x_{0i}})(\hat{c}_0\cos\varphi_i-\hat{u}_0)+(\Delta_{y_i}-\Delta_{y_{0i}})\times(\hat{c}_0\sin\varphi_i-\hat{v}_0)+(L_i-2\hat{c}_0t_i^{\mathrm{tr}})\Delta_{c_0}-L_i(\Delta_{u_0}\cos\varphi_i+\Delta_{v_0}\sin\varphi_i)-\hat{c}_0^2\Delta_{t_i},\tag{34}$$

and, as $\hat{u}_0\ll\hat{c}_0$, $\hat{v}_0\ll\hat{c}_0$, and $\hat{c}_0t_i^{\mathrm{tr}}\sim L_i$, the variance $\sigma_{q_i}^2=\langle\Delta_{q_i}^2\rangle$ of the errors in q_i is

$$\sigma_{q_i}^2\approx 2\sigma_r^2\hat{c}_0^2+L_i^2(\hat{\sigma}_c^2+\hat{\sigma}_u^2\cos^2\varphi_i+\hat{\sigma}_v^2\sin^2\varphi_i)+\hat{c}_0^4\sigma_t^2,\tag{35}$$

where σ_r^2 is the variance of the errors in the transducer positions ($\sigma_r^2=\langle\Delta_{x_i}^2\rangle=\langle\Delta_{x_{0i}}^2\rangle=\langle\Delta_{y_i}^2\rangle=\langle\Delta_{y_{0i}}^2\rangle$), and σ_t^2 is the variance of an error in measurement of t_i^{tr}.

V. ACOUSTIC TOMOGRAPHY EXPERIMENT

In this section, a developed theory of TDSI is applied to reconstruction of temperature $\tilde{T}$ and wind velocity $\tilde{\mathbf{V}}$ fields in the acoustic tomography experiment STINHO carried out by scientists from the University of Leipzig.[9] The experiment was a part of a larger meteorological experiment to study turbulence, turbulent fluxes, and other meteorological parameters over heterogeneous surface.

The tomography array consisted of eight sources $\mathrm{S1},\ldots,\mathrm{S8}$ and twelve receives $\mathrm{R1},\ldots,\mathrm{R12}$, see Fig. 1. The size of the array was 300 m × 440 m. The sources and receivers were located above the ground at an average height of 2 m. Most of the ground within the tomography array was covered with grass except for a spot of bare soil which was in the lower left corner of the array with the size of 90 m × 300 m. This inhomogeneity might create the fluctuation of

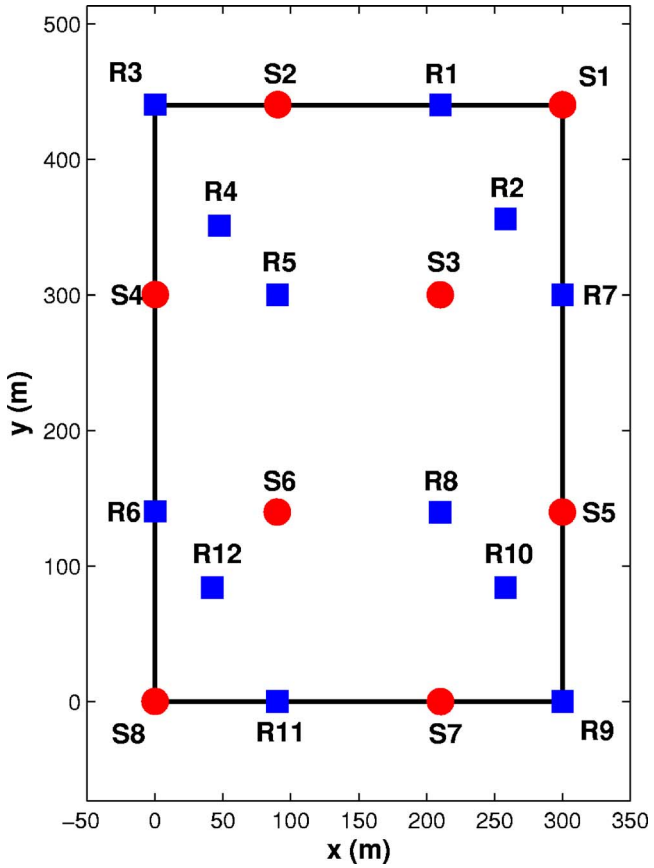

FIG. 1. (Color online) The layout of sources (S1,...,S8) and receivers (R1,...,R12) in the acoustic tomography experiment STINHO (Ref. 9).

temperature and wind velocity fields which is subject of reconstruction by TDSI. Besides, the difference between mean temperatures over different surfaces was negligible (unlike the difference in turbulent heat fluxes), and horizontal wind velocities were quite close (see Fig. 2 in the Ref. 9). The travel times t_i^{tr} of sound propagation between sources and receivers were measured every minute during 6 July 2002.

Our reconstruction of temperature $\tilde{T}$ and wind velocity $\tilde{\mathbf{V}}$ fields in this acoustic tomography experiment consisted in reconstruction of their mean values $\hat{T}_0(t)$, $\hat{u}_0(t)$, and $\hat{v}_0(t)$ and fluctuations $\hat{T}(\mathbf{R},t)$, $\hat{u}(\mathbf{R},t)$, and $\hat{v}(\mathbf{R},t)$ as described in Sec. II. The input experimental data for reconstruction of $\hat{T}_0(t)$, $\hat{u}_0(t)$, and $\hat{v}_0(t)$ were t_i^{tr}, L_i, and φ_i. The reconstructed mean values of temperature and two components of wind velocity for the 10 min time interval (5:26–5:35 a.m., Coordinated Universal Time (UTC), which is also known as Greenwich Mean Time) are plotted in Fig. 2 as solid lines. Using Eq. (32), the errors $\hat{\sigma}_T$, $\hat{\sigma}_u$, and $\hat{\sigma}_v$ in reconstruction of the mean fields were calculated. These errors are plotted in Fig. 2 as vertical bars.

Then, the obtained values of $\hat{T}_0(t)$, $\hat{u}_0(t)$, and $\hat{v}_0(t)$ and experimental values of t_i^{tr} were used to calculate the components $q_i(t)$ of the input data $\mathbf{d}$ for reconstruction of fluctuations $\hat{T}(\mathbf{R},t)$, $\hat{u}(\mathbf{R},t)$, and $\hat{v}(\mathbf{R},t)$ using TDSI. To apply TDSI, we also needed to know the variances $\sigma_{q_i}^2$ of errors in $q_i(t)$, and parameters σ_T, σ_V, l_T, and l_V of the covariance functions $B_{TT}(\boldsymbol{\rho},\tau)$ and $B_{ij}(\boldsymbol{\rho},\tau)$. The variances $\sigma_{q_i}^2$ were calculated using Eq. (35), where $\hat{\sigma}_c^2$, $\hat{\sigma}_u^2$, and $\hat{\sigma}_v^2$ were obtained from Eq. (32), whereas σ_r^2 and σ_t^2 were estimated in the tomography experiment[9] to be as follows: $\sigma_r=3$ cm and $\sigma_t=0.3$ ms. The variances of temperature and velocity fluctuations, σ_T and σ_V, were assumed to be the same as the variances measured *in situ* by a sonic thermometer-anemometer: $\sigma_T=0.27\,^{\circ}\mathrm{C}$ and $\sigma_V=0.28$ m/s. The correlation lengths l_T and l_V were chosen as follows: $l_T=l_V=75$ m. The values of l_T and l_V determine a characteristic size of fluctuations $\hat{T}(\mathbf{R},t)$, $\hat{u}(\mathbf{R},t)$, and $\hat{v}(\mathbf{R},t)$ which can be resolved in reconstruction. Note that, for the considered experiment, the values of l_T and l_V could not be chosen significantly less than 75 m since the errors in reconstruction of the fluctuations increase with decreasing l_T and l_V.[13] Finally, to apply TDSI to the reconstruction of the fluctuations $\hat{T}(\mathbf{R},t)$, $\hat{u}(\mathbf{R},t)$, $\hat{v}(\mathbf{R},t)$, three con-

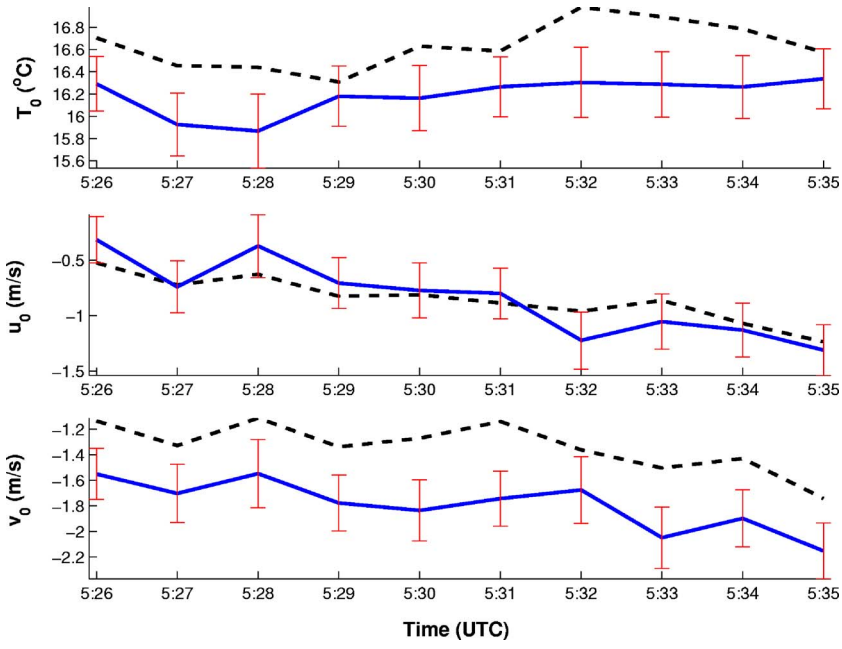

FIG. 2. (Color online) The reconstruction of the mean fields at 5:26–5:30 a.m. UTC on 6 July 2002 by TDSI (solid lines) and SIRT (dashed lines). The vertical bars indicate the estimated errors of mean field reconstruction by TDSI.

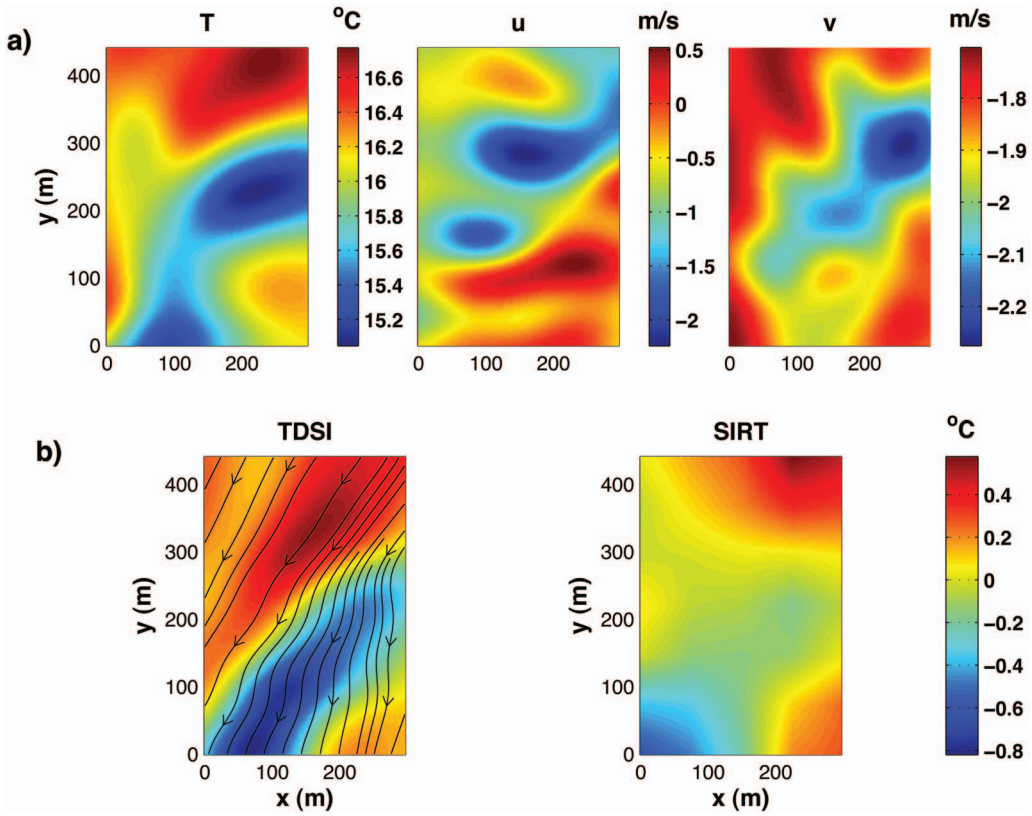

FIG. 3. (a) The TDSI reconstruction of temperature (°C) and wind velocity (m/s) fields at 5:30 a.m. UTC on 6 July 2002. (b) The 10 min averaged fields of temperature fluctuations (°C) reconstructed by (left) TDSI and (right) SIRT. The black lines in the TDSI reconstruction show the direction of reconstructed mean wind during the interval of averaging.

secutive sets of the travel times t_i^{tr} were used. (In future tomography experiments, it would be desirable to increase the number of such sets by decreasing a time interval between measurements of t_i^{tr}). After the fluctuations $\hat{T}(\mathbf{R},t)$, $\hat{u}(\mathbf{R},t)$, and $\hat{v}(\mathbf{R},t)$ were reconstructed, the total fields $\tilde{T}$, $\tilde{u}$, and $\tilde{v}$ were obtained as the sums of the mean fields and fluctuations.

Figure 3(a) shows the fields $\tilde{T}$, $\tilde{u}$, and $\tilde{v}$ reconstructed at 5:30 a.m. UTC (In the reconstruction, the travel times t_i^{tr} measured at 5:29, 5:30, and 5:31 a.m. were used.) "Cold" and "warm" temperature eddies with different scales can be seen in Fig. 3(a). High and low speed velocity eddies can also be seen. Figure 4 contains the expected root mean squared errors (RMSE) of the reconstruction of temperature and wind velocity fields shown in Fig. 3(a). These errors are calculated with the use of Eq. (16). The spatially averaged RMSE of temperature reconstruction is 0.36 °C. This error is less than the temperature differences between cold and warm eddies which can be seen in Fig. 3(a). Therefore, these cold and warm eddies are reliably reconstructed. The spatially averaged RMSE of $\tilde{u}$ and $\tilde{v}$ reconstruction are 0.35 and 0.25 m/s, respectively. These errors are also less than the velocity differences between the low and high speed eddies which can be seen in Fig. 3(a).

The reconstructed values of temperature were compared with those measured by two in-situ sensors located within the tomographic area. The results of this comparison and the coordinates of the sensors are presented in Table I. According to Table I, the reconstructed values of temperature are in a good agreement with the direct measurements: The discrepancy is 0.1 °C at the location of the first sensor and 0.01 °C at the location of the second sensor. These discrepancies are smaller than the estimated errors of the reconstruction, which are of order 0.4 °C.

For the considered tomography experiment, the temperature and wind velocity fields were also reconstructed in Ref. 9 using a Simultaneous Iterative Reconstruction Technique (SIRT) algorithm. SIRT is an algebraic algorithm which does not use *a priori* information about covariance functions of turbulent fields. It is worthwhile to compare the results presented in Ref. 9 with those obtained by TDSI. Note that the SIRT algorithm used in Ref. 9 is also a two step procedure. In the first step, the travel times t_i^{tr} are split into t_{iT}^{tr} and t_{iV}^{tr}, where t_{iT}^{tr} are affected only by the temperature field $\tilde{T}$, whereas t_{iV}^{tr} are affected only by the velocity field $\tilde{\mathbf{V}}$ (for details see Ref. 8). In the second step, the SIRT algorithm is used to reconstruct the temperature and velocity fields from t_{iT}^{tr} and t_{iV}^{tr}, respectively. In Fig. 2, the dashed lines correspond to the mean values of the temperature and two components of wind velocity reconstructed by SIRT. Comparison of these lines with the solid ones (obtained by TDSI) shows that there is an acceptable agreement in reconstruction of $\hat{T}_0(t)$, $\hat{u}_0(t)$, and $\hat{v}_0(t)$ by two algorithms. The root mean squared discrepancy between values obtained by SIRT and TDSI is 0.47 °C for the $\hat{T}_0$, 0.16 m/s for the $\hat{u}_0$, and 0.47 m/s for the $\hat{v}_0$.

TABLE I. Comparison of the reconstructed and *in situ* measured values of temperature.

Landscape type	Coordinated (m)	Humitter T (°C)	TDSI T (°C)
Bare soil	$x=28$, $y=138$	16.24	16.14
Grassland	$x=182$, $y=143$	15.78	15.77

Figure 3(b) shows the temperature fluctuations $\hat{T}$ averaged over 10 min and reconstructed with the use of TDSI and SIRT. The SIRT reconstruction of $\hat{T}$ was taken from Ref. 9 (see Fig. 4 in that reference) and then the temperature field was interpolated (2D linear interpolation) to have the same spatial grid as that used in TDSI. It follows from Fig. 3(b) that the reconstructed fields are similar on large scales of turbulent eddies. In the lower left-hand corner of Fig. 3(b), one can see a cold temperature eddy which is stretched at about 45° with respect to the x axis. Further, there are two warm eddies in the right upper and lower corners. However, there are differences in the reconstructed fields in details. According to the TDSI reconstruction, the cold eddy in the left lower corner is more distinctive, narrower and longer than that reconstructed by SIRT. The shape of the warm eddy in the upper right-hand corner is also more stretched along the diagonal and centered at a different position. It is worthwhile to note that, in TDSI, the deformation of the turbulent eddies along the diagonal coincides with the direction of reconstructed mean wind during the interval of averaging [black lines in Fig. 3(b), left plot].

The estimated RMSE for the TDSI and SIRT reconstructions are shown in Fig. 5. Note that the errors of the reconstruction by TDSI are of order 0.1 °C, and are approximately one-half the SIRT errors.

VI. CONCLUSIONS

In this paper, the TDSI methodology for acoustic tomography of the atmosphere was further developed. First, the formulas for the spatial-temporal covariance functions of temperature and wind velocity fluctuations for the case of locally frozen turbulence were derived. These formulas are more general than those for the case of frozen turbulence and account for the variance of velocity fluctuations. Second, the formulas for the variances of the errors in the input data in TDSI were derived.

The developed TDSI was, for the first time, used in the reconstruction of temperature and wind velocity fields in an acoustic tomography of the atmosphere experiment (STINHO experiment[9]). The reconstructed temperature and wind velocity fields and the errors in the reconstruction were presented. It was shown that the use of TDSI allowed us to reliably reconstruct temperature and velocity eddies within the tomographic area. The temperature field reconstructed by TDSI was compared with that reconstructed by the SIRT method. The fields reconstructed by these two approaches are similar on large scales while different in details. TDSI yields a more detailed reconstruction with the errors in about one-half those in SIRT.

Note that the STINHO experiment was not designed to take the full advantages of TDSI. In future experiments, it is worthwhile to fully exploit these advantages. For example, it would be worthwhile to reduce the time intervals between consecutive travel time measurements.

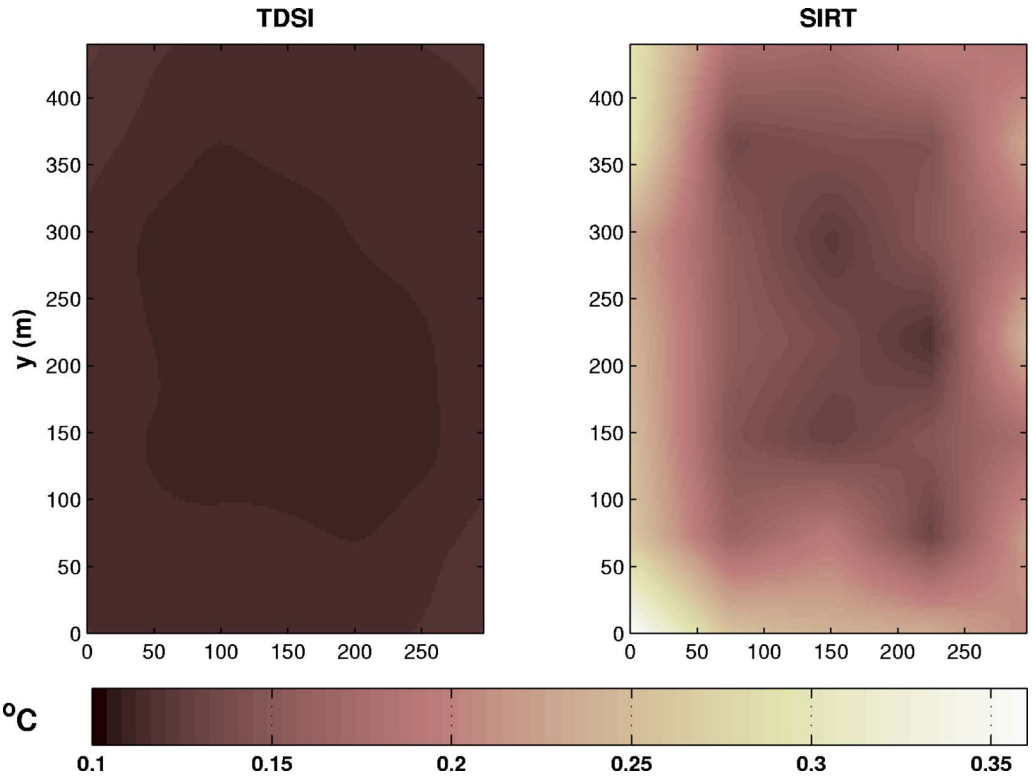

FIG. 5. (Color online) The expected root mean squared errors in the reconstructions shown in Fig. 3(b).

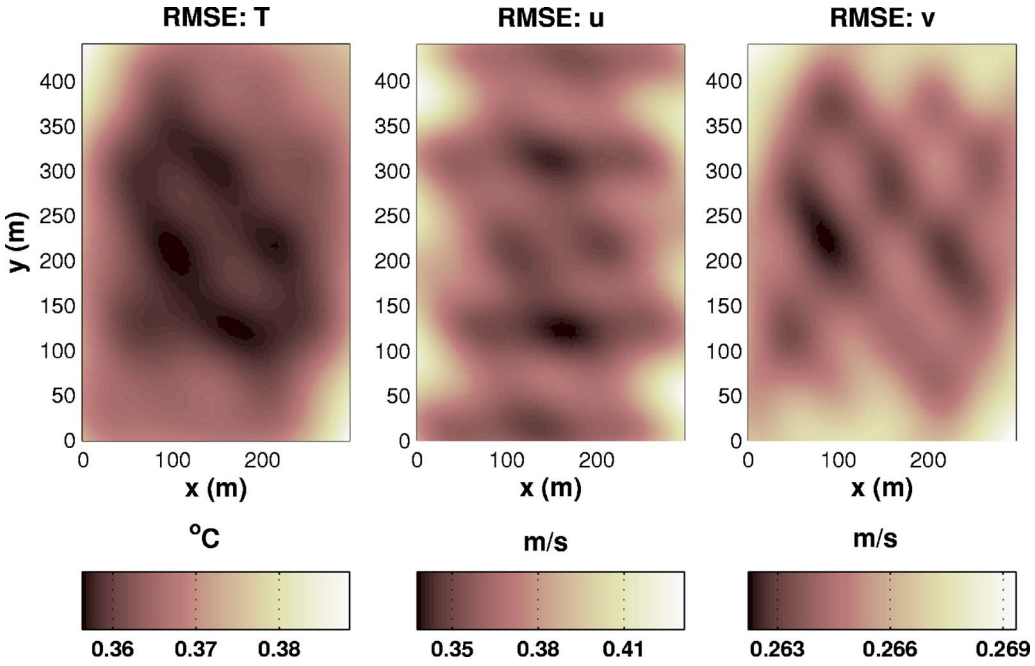

FIG. 4. (Color online) The expected root mean squared errors in the reconstructions shown in Fig. 3(a).

ACKNOWLEDGMENTS

This material is partly based upon work that was supported by the U.S. Army Research Office under Contract Nos. DAAD19-03-1-0104 and W911NF-06-1-0007. The STINHO project was performed as a part of the VERTICO (VERTIcal transports of energy and trace gases at anchor stations under COmplex natural conditions) network which was funded by the German Federal Ministry of Education and Research (BmBF) in the framework of the AFO-2000 research program (Grant No. 07ATF37).

APPENDIX: SPATIAL-TEMPORAL COVARIANCE FUNCTION FOR LOCALLY FROZEN TURBULENCE

In this appendix, we derive a formula for the spatial-temporal covariance function of temperature fluctuations for the case of locally frozen turbulence. A starting equation for this derivation is Eq. (22). Substituting the value of B_{TT}^s from Eq. (17) into Eq. (22), we have

$$B_{TT}(\boldsymbol{\rho},\tau)=\sigma_T^2\left\langle \exp\left(-\frac{(\rho_x-\tilde{u}\tau)^2}{l_T^2}-\frac{(\rho_y-\tilde{v}\tau)^2}{l_T^2}-\frac{(\rho_z-\tilde{w}\tau)^2}{l_T^2}\right)\right\rangle_{\tilde{\mathbf{V}}}. \tag{A1}$$

We will assume that the random 3D field $\tilde{\mathbf{V}}(\mathbf{R},t)$ is normally distributed with the variance $\sigma_{\tilde{\mathbf{V}}}^2$ independent of spatial coordinates and time: $\sigma_{\tilde{\mathbf{V}}}^2=\langle\tilde{\mathbf{V}}^2(\mathbf{R},t)\rangle=\langle u^2(\mathbf{R},t)\rangle+\langle v^2(\mathbf{R},t)\rangle+\langle w^2(\mathbf{R},t)\rangle=3\sigma_V^2$. Its mathematical expectation is $\mathbf{V}_0(t)=(u_0(t),v_0(t),w_0(t))$. Note that different components of $\tilde{\mathbf{V}}(\mathbf{R},t)$ are uncorrelated in the theory of homogeneous isotropic turbulence which is used in this paper. Indeed, as turbulence is stationary, at any time t the cross correlations between two different components of $\tilde{\mathbf{V}}$, e.g., $\tilde{u}$ and $\tilde{v}$, are described by B_{uv}^s given by Eq. (19). It follows from this equation that the cross correlation at a fixed point ($\rho_x=\rho_y=\rho_z=0$) is equal to zero. If components of a multidimensional normally distributed variable are uncorrelated then they are independent. Statistical independence of different components of $\tilde{\mathbf{V}}(\mathbf{R},t)$ allows one to express Eq. (A1) in the following form:

$$B_{TT}(\boldsymbol{\rho},\tau)=\sigma_T^2 I_x I_y I_z, \tag{A2}$$

where $I_x=\langle\exp[-(\rho_x-\tilde{u}\tau)^2/l_T^2]\rangle_{\tilde{u}}$, and I_y and I_z are given by similar formulas. Let $\eta=(\rho_x-\tilde{u}\tau)/l_T$. Then I_x can be written as $I_x=\langle\exp(-\eta^2)\rangle_\eta$. Note that a random function η is normally distributed as ρ_x, l_T, and τ are nonrandom quantities and $\tilde{u}$ is a normally distributed random function. Therefore, η has a Gaussian probability density

$$p_\eta(w)=\frac{1}{\sigma_\eta\sqrt{2\pi}}\exp\left[-\frac{(w-\langle\eta\rangle)^2}{2\sigma_\eta^2}\right]$$

with its mean value $\langle\eta\rangle$ and variance σ_η^2 given by

$$\langle\eta\rangle=\frac{\rho_x-u_0(t_1)\tau}{l_T},\quad \sigma_\eta^2=\frac{\sigma_V^2\tau^2}{l_T^2} \tag{A3}$$

Then

$$I_x=\int_{-\infty}^{\infty}\exp(-w^2)p_\eta(w)dw=\frac{1}{\sqrt{1+2\sigma_\eta^2}}\exp\left(\frac{\langle\eta\rangle^2}{1+2\sigma_\eta^2}\right). \tag{A4}$$

Similar results can be obtained for I_y and I_z. Substituting Eq. (A4) and similar formulas for I_y and I_z into Eq. (A2), we obtain an analytical formula for $B_{TT}(\boldsymbol{\rho},\tau)$. This formula is given by Eq. (23).

[1]J. L. Spiesberger and K. M. Fristrup, "Passive localization of calling animals and sensing of their acoustic environment using acoustic tomogra-

phy," Am. Nat. **135**, 107–153 (1990).
[2]D. K. Wilson and D. W. Thomson, "Acoustic tomographic monitoring of the atmospheric surface layer," J. Atmos. Ocean. Technol. **11**, 751–769 (1994).
[3]A. Ziemann, K. Arnold, and A. Raabe, "Acoustic tomography in the atmospheric surface layers," Ann. Geophys. **17**, 139–148 (1999).
[4]K. Arnold, A. Ziemann, and A. Raabe, "Acoustic tomography inside the atmospheric boundary layer," Phys. Chem. Earth, Part B **24**, 133–137 (1999).
[5]A. Ziemann, K. Arnold, and A. Raabe, "Acoustic travel-time tomography—a method for remote sensing of the atmospheric surface layer," Meteorol. Atmos. Phys. **71**, 43–51 (1999).
[6]A. Ziemann, K. Arnold, and A. Raabe, "Acoustic tomography as a method to identify small-scale land surface characteristic," Acta. Acust. Acust. **87**, 731–737 (2001).
[7]K. Arnold, A. Ziemann, and A. Raabe, "Tomographic monitoring of wind and temperature at different heights above the ground," Acta. Acust. Acust. **87**, 703–708 (2001).
[8]A. Ziemann, K. Arnold, and A. Raabe, "Acoustic tomography as a remote sensing method to investigate the nearsurface atmospheric boundary layer in comparison with in situ measurements," J. Atmos. Ocean. Technol. **19**, 1208–1215 (2002).
[9]A. Raabe, K. Arnold, A. Ziemann, M. Schröter, S. Raasch, J. Bange, P. Zittel, Th. Spieb, Th. Foken, M. Göckede, F. Beyrich, and J.-P. Leps, "STINHO–STructure of turbulent transport under INHOmogeneous surface conditions - a micro-α scale field experiment and LES modeling," Meteorol. Z. **14**, 315–327 (2005).
[10]D. K. Wilson, A. Ziemann, V. E. Ostashev, and A. G. Voronovich, "An overview of acoustic travel-time tomography in the atmosphere and its potential applications," Acta. Acust. Acust. **87**, 721–730 (2001).
[11]S. L. Collier, D. A. Ligon, J. M. Noble, E. Patton, P. Sullivan, and V. E. Ostashev, "Acoustic tomographic array simulation," *Proceedings of the 11th International Symposium on Long Range Sound Propagation*, Fairlee, VT, 2004.
[12]S. N. Vecherin, V. E. Ostashev, D. K. Wilson, A. G. Voronovich, G. H. Goedecke, S. L. Collier, J. M. Noble, and D. Ligon, "Forward and inverse problems of acoustic tomography of the atmosphere," *Proceedings of the 11th International Symposium on Long Range Sound Propagation*, Fairlee, VT, 2004.
[13]D. K. Wilson, V. E. Ostashev, S. N. Vecherin, A. G. Voronovich, S. L. Collier, and J. M. Noble, "Assessment of acoustic travel-time tomography of the atmospheric surface layer," *Proceedings of AMS Symposium on Boundary Layers and Turbulence*, Portland, ME, 2004.
[14]P. Holstein, A. Raabe, R. Müller, M. Barth, D. Mackenzie, and E. Starke, "Acoustic tomography on the basis of travel-time measurement," Meas. Sci. Technol. **15**, 1420–1428 (2004).
[15]M. Barth, A. Raabe, P. Holstein, R. Muller, A. Ziemann, K. Arnold, D. Mackenzie, E. Starke, and M. Seliger, "Acoustic travel-time tomography as a tool to investigate temperature distributions on different spatial scales," *12th International Symposium on Acoustic Remote Sensing and Associated Techniques of the Atmosphere and Oceans*, Cambridge, United Kingdom, 2004.
[16]K. Aki and P. G. Richards, *Quantitative Seismology. Theory and methods* (Freeman, San Francisco, 1980).
[17]V. E. Ostashev, S. N. Vecherin, D. K. Wilson, and S. L. Collier, "Correlation functions of temperature and velocity fluctuations in a turbulent atmosphere," J. Acoust. Soc. Am. **119**, 3264 (2006).
[18]V. E. Ostashev, *Acoustics in Moving Inhomogeneous Media* (E&FN SPON, London, 1997).
[19]S. N. Vecherin, V. E. Ostashev, G. H. Goedecke, D. K. Wilson, and A. G. Voronovich, "Time-dependent stochastic inversion in acoustic travel-time tomography of the atmosphere," J. Acoust. Soc. Am. **119**, 2579–2588 (2006).
[20]J. Hinze, *Turbulence* (McGraw-Hill, New York, 1975).
[21]J. Gilson, D. Roemmich, B. D. Cornuelle, and L.-L. Fu, "Relationship of TOPEX/Poseidon altimetric height to steric height and circulation in the North Pacific," J. Geophys. Res. **103**, 27947–27965 (1998).
[22]N. Ducet, P. Y. Le Traon, and G. Reverdin, "Global high-resolution mapping of ocean circulation from TOPEX/Poseidon and ERS-1 and -2," J. Geophys. Res. **105**, 19477–19498 (2000).
[23]F. P. Bretherton, R. E. Davis, and C. B. Fandry, "A technique for objective analysis and design of oceanographic experiments applied to MODE-73," Deep-Sea Res. **23**, 559–582 (1976).
[24]V. I. Tatarskii, *The Effects of the Turbulent Atmosphere on Wave Propagation* (Keter, Jerusalem, 1971).